Inorg. Chem. **2005**, *44*, 7781–7793

Electronic Structure of $M(BH_4)_4$, M = Zr, Hf, and U, by Variable Photon-Energy Photoelectron Spectroscopy and Density Functional Calculations

Jennifer C. Green,*,† Monica de Simone,‡ Marcello Coreno,§ Aled Jones,|| Helen M. I. Pritchard,|| and G. Sean McGrady⊥

Inorganic Chemistry Laboratory, University of Oxford, South Parks Road, Oxford OX1 3QR, UK, CNR−Laboratori Nationali TASC−INFM, I-34012 Basovizza, Trieste, Italy, CNR−IMIP, Area della Ricerca di Roma,CP10, I-00016 Monterotondo Scalo, Italy, Department of Chemistry, King's College London, Strand, London, WC2R 2LS UK, and Department of Chemistry, University of New Brunswick, Fredericton, N.B. E3B 6E2, Canada

Received March 10, 2005

Photoelectron (PE) spectra have been obtained for the $M(BH_4)_4$ (M = Zr, Hf and U) molecules in the 20–60 eV photon-energy range, and for M = U, also in the 90–120 eV region. Derived branching ratios (BR) and relative partial-photoionization cross sections (RPPICS) of the valence bands are used to confirm band assignment and demonstrate d-orbital covalency for all three compounds and f-orbital covalency for $U(BH_4)_4$. Core ionizations are identified and used to confirm resonance features in the RPPICS. The absorption spectrum of $Zr(BH_4)_4$ between 20 and 60 eV shows 4p absorption at 35.5 eV, coincident with the 4p–4d resonance in the RPPICS of the 1e and $2t_2$ ionization bands of $Zr(BH_4)_4$. Less intense absorption bands at 32.5 and 33.8 eV correspond with shape resonance features in the $1a_1$ and $1t_2$ PE bands. The RPPICS of the f band of $U(BH_4)_4$ shows two strong resonant features between 95 and 120 eV. Direct photoemission of the 5f electrons from $U(BH_4)_4$ results only in the observation of the $^2F_{5/2}$ ion state of $[U(BH_4)_4]^+$, but in the 5d–5f resonant region, a weak band corresponding to the $^2F_{7/2}$ ion state is also observed. The splitting of the $1t_2$ band of $U(BH_4)_4$ is attributed to a small contribution of U 6p semi-core electrons to this MO. Density functional calculations give a good estimate of the pattern of ionization energies, although the calculated absolute values are lower than the experimental values, the first IE by 0.5 eV for $Zr(BH_4)_4$ and $Hf(BH_4)_4$ and 1.0 eV for $U(BH_4)_4$. The MO compositions are in very good agreement with the deductions made from the BR and RPPICS analyses.

Introduction

Although the capacity of s, p, and d orbitals to form covalent bonds in inorganic molecules is well documented, the role of f orbitals in bonding is more controversial.[1−3] In lanthanide and actinide complexes, the energies of the f orbitals place them in the valence region but their radial distribution, as a consequence of their low principal quantum number, is corelike, and their high angular momentum bequeaths nodal properties that can result in a modest overlap with ligand orbitals.

One of the most direct experimental methods of studying the atomic orbital (AO) composition of molecular orbitals (MOs) is variable photon-energy photoelectron (PE) spectroscopy.[4−6] The relative partial-photoionization cross section (RPPICS) of a PE band shows features which may be attributed to the AOs from which the originating MO is composed. For example, the closeness of a RPPICS maximum to threshold is a function of the angular momentum of

* To whom correspondence should be addressed. E-mail: jennifer.green@chem.ox.ac.uk.
† University of Oxford.
‡ CNR−Laboratori Nationali TASC−INFM.
§ CNR-IMIP.
|| King's College London.
⊥ University of New Brunswick.

(1) Denning, R. G. *Struct. Bonding (Berlin)* **1992**, *79*, 215.
(2) Li, J.; Bursten, B. E. *J. Am. Chem. Soc.* **2004**, *119*, 9021.
(3) Denning, R. G.; Green, J. C.; Hutchings, T. E.; Dallera, C.; Tagliaferri, A.; Giarda, K.; Brookes, N. B.; Braicovich, L. *J. Chem. Phys.* **2002**, *117*, 8008.
(4) Green, J. C. *Acc. Chem. Res.* **1994**, *27*, 131.
(5) Green, J. C.; Decleva, P. *Coord. Chem. Rev.* **2004**, *249*, 209.
(6) Solomon, E. I.; Basumallick, L.; Chen, P.; Kennepohl, P. *Coord. Chem. Rev.* **2005**, *249*, 229.

10.1021/ic050370u CCC: $30.25
Published on Web 10/04/2005

the AO, with d and f orbitals exhibiting delayed maxima. Furthermore, AOs with radial nodes show Cooper minima, which are useful in distinguishing the s and p bands with principal quantum numbers higher than 1 or 2, respectively. Most dramatically, d and f ionizations may be significantly enhanced by a resonant process, whereby an inner shell p or d electron undergoes an excitation into a vacant orbital of d or p character followed by a super Coster−Kronig decay, resulting in the ejection of a bound d or f electron. The photon energy at which these various features occur is predictable to within a few electronvolts, so the overall RPPICS profile may be analyzed productively. This technique has established f-orbital covalency in the molecule uranocene, $(\eta^8\text{-}C_8H_8)_2U$.[7] Complications arise in the interpretation of intensity changes because, at low photon energies, other processes give rise to BR and RPPICS variations; these include shape resonances, which are molecular rather than atomic in origin. Thus, precise identification of the energies of relevant core ionizations of the molecule assist in the firm assignment of features. Ideally, the measurement of the absorption spectra in the VUV region would give information on the various resonance processes.

The series of volatile tetrahedral molecules, $M(BH_4)_4$ (M = Zr, Hf, and U), offers a unique opportunity to undertake a comparative bonding study. The heavy-atom MB_4 skeleton conforms to T_d symmetry in each case, and the MO scheme and PE spectra can be interpreted in this point group. Accordingly, the ligand symmetry-adapted linear combinations (SALCs) span the representations a_1, e, t_2, and t_1. Only an f orbital can provide a symmetry match for the t_1 combination.

He I and He II spectra of all three compounds have been measured previously,[8,9] as has that of $Th(BH_4)_4$.[10] The two reports of the Zr and Hf compounds showed identical spectra, but differed in their assignments. Downs et al.[8] based their interpretation on localized orbitals for the bridging M−H−B and terminal B−H bonds, arguing that the terminal ones had the lower ionization energy (IE). Subsequent work reassigned the spectra with the aid of LCAO−HFS(Xα) calculations.[9] These suggested that the t_1 orbital was the HOMO and was associated with the lowest IE band. PE studies of $M(BH_3Me)_4$ (M = Zr, Hf, Th and U), where a methyl group has replaced the terminal B−H bond, confirmed the assignment of the first band for the transition metal species as a t_1 ionization. Associated Xα-SW calculations also suggested that for the actinide derivatives the HOMO was t_2 in symmetry, with the t_1 orbitals being more stable as a result of a modest bonding interaction with the actinide 5f orbitals.[11] One aim of the current study, therefore, was to seek experimental evidence for this f-orbital covalency in $U(BH_4)_4$.

Experimental Section

Synthesis. The metal tetrakis-borohydrides, $M(BH_4)_4$ (M = Zr, Hf and U), were prepared by an adaptation of the original method described by Wallbridge et al.,[12,13] involving a solvent-free reaction between MCl_4 and an excess of freshly recrystallized $LiBH_4$. The resulting $M(BH_4)_4$ product was purified in each case by sublimation in vacuo and stored in a Pyrex glass ampule closed with a Teflon valve (J. Young, London).

PE Spectra. Measurements were carried out on the undulator-based Gas-Phase Photoemission beamline at ELETTRA, Trieste,[14] using the ARPES chamber and an ionization cell.[15] The monochromator was a VASGM (Variable-Angle Spherical-Grating Monochromator), working with four gratings to cover the energy range of 20−1200 eV, with a photon-energy resolution $\Delta E/E \leq 10\,000$. Consequently, the He and Ar signals typically had full width at half-maximum (fwhm) values of 0.11 eV. The PE spectra were normalized using the signal from a calibrated photodiode (IRD, Inc.), while the absorption spectra were normalized to the signal of the incoming photon flux detected by a gold mesh.

$Zr(BH_4)_4$ and $Hf(BH_4)_4$ are highly volatile, and $U(BH_4)_4$ is somewhat less so. The samples, contained in Pyrex ampules wrapped in aluminum foil, were held under vacuum at room-temperature external to the spectrometer, and their vapor was introduced into the chamber via a needle valve and 4 mm tube close to the ionization region. Either He or Ar was simultaneously introduced with the sample in order to calibrate the intensity measurements. He has the advantage of the higher cross section above 30 eV, but only Ar can be used to calibrate the spectra between 20 and 30 eV because of the high IE of He. Both gases were used for $Zr(BH_4)_4$. For $Hf(BH_4)_4$, the He band coincided with a core signal, so only Ar was employed. For $U(BH_4)_4$, Ar was used for the photon-energy range of 20−50 eV, and He was used for the photon-energy range of 90−125 eV.

We have to stress that $U(BH_4)_4$ had a deleterious effect on the electron detector: upon exposure to the vapor, the detector lost sensitivity. Upon removal of the sample and pumping, it recovered to a certain extent, but not completely. An increase in the channeltron voltage helped to recover signal. We solved the problem through a co-flowing stream of He or Ar that slowed the rate of the decline and made data collection possible, but never easy.

The ARPES chamber was equipped with a 50 mm mean-radius electron-energy analyzer (VSW Ltd.) mounted at the magic angle. Pass energies of 5 and 10 eV were used for valence-PE spectra. Core and inner valence spectra were recorded using a pass energy of 10 eV. The overall gas pressure was held at about 1×10^{-5} mbar.

The PE spectra of the valence region (from 8 to 21 eV binding energy) were measured at the magic angle for a series of photon energies ranging from 20 to 60 eV for all three molecules using grating 1 (400 l/mm), and for $U(BH_4)_4$ between 67 and 110 eV, using grating 3 (1200 l/mm). B 1s ionizations were measured using grating 4 and a photon energy of 244.37 eV. Zr 4p and Hf 4f and 5p bands were measured using a photon energy of 60 eV, and the U 6p bands were measured with a photon energy of 45 eV.

(7) Brennan, J. G.; Green, J. C.; Redfern, C. M. *J. Am. Chem. Soc.* **1989**, *111*, 2373.
(8) Downs, A. J.; Egdell, R. G.; Orchard, A. F.; Thomas, P. D. P. *J. Chem. Soc., Dalton Trans.* **1978**, 1755.
(9) Hitchcock, A. P.; Hao, N.; Werstiuk, N. H.; McGlinchey, M. J.; Zeigler, T. *Inorg. Chem.* **1982**, *21*, 793.
(10) Green, J. C.; Shinomoto, R.; Edelstein, N. *Inorg. Chem.* **1986**, *25*, 2718.
(11) Hohl, D.; Rösch, N. *Inorg. Chem.* **1986**, *25*, 2711.
(12) Davies, N.; Saunders, D.; Wallbridge, M. G. H. *J. Chem. Soc. A* **1970**, 2915.
(13) Haaland, A.; Shorokhov, D. J.; Tutukin, A. V.; Volden, H. V.; Swang, O.; McGrady, G. S.; Kaltsoyannis, N.; Downs, A. J.; Tang, C. Y.; Turner, J. F. C. *Inorg. Chem.* **2002**, *41*, 6646.
(14) Prince, K. C.; Blyth, R. R.; Delaunay, R.; Zitnik, M.; Krempasky, J.; Slezak, J.; Camilloni, R.; Avaldi, L.; Coreno, M.; Stefani, G.; C. Furlani; de Simone, M.; Stranges, S. *J. Sync. Rad.* **1998**, *5*, 565.
(15) Fronzoni, G.; de Simone, M.; Coreno, M.; Prince, K. C.; Furlan, S.; Franceschi, P.; Decleva, P. *Phys. Chem. Chem. Phys.* **2003**, *5*, 2758.

A Zr 4p edge-region absorption spectrum was measured over the photon-energy range of 24−60 eV using grating 1, with a photon-energy bandwidth varying from 3 to 10 meV. The acquisition in this photon-energy range was possible through the parallel scan of the undulator gap and the dispersed wavelength from VASGM. Normalization of data using the electron yield from a gold mesh before the interaction region, resulted in complete removal of the wiggles caused by the sawtooth shape of I_0.

Branching ratios, BR, give the ratio of band intensities as a function of photon energy. They are commonly normalized so that the sum of the BR for all included bands comes to 1. A photoelectron cross section is proportional to the probability of photoionization to a particular ion state. It depends on the photon energy and on the angle of detection of the photoelectron with respect to the direction of propagation of the photons and their polarization. There is a magic angle ($3\cos^2\theta = 1$), at which the partial-photoionization cross section (PPICS) is proportional to the total-integrated cross section and independent of an angular parameter, β. Measurements were made at this angle. In this work, there is no measure of the pressure of the sample gas at the point of ionization, hence the derived partial-photoionization cross sections are relative rather than absolute and are denoted RPPICS. The units are consequently arbitrary.

To obtain BR and RPPICS for the various valence bands, the data points were divided by the beam intensity, measured during the course of a run by a photomultiplier positioned after the ionization region in the path of the beam. The normalized spectra at each photon energy were compared for consistency and converted into a time-weighted average spectrum. Spectra were then fitted with Gaussian peaks using the routine available in IGOR Pro (WaveMatrix Inc.) with background subtraction. BR values were available directly from the areas of the Gaussian peaks. RPPICS values were obtained using the He or Ar calibration data. The measured band intensities were multiplied by the ratio I_{abs}/I_{exp} to correct for instrumental bias.

Errors. Instrumental factors that could give rise to errors in branching ratios were treated in the following manner. The variation in the beam flux was monitored by the photodiode and used to produce a spectrum with normalized counts as discussed above. The sample pressure was held constant by controlling the sample temperature and monitoring the chamber pressure. The sample pressure was checked over time by repeated monitoring of the sample spectrum at a fixed photon energy. For RPPICS measurements, other factors are important and were taken into account by the simultaneous measurement of a inert gas with every spectrum. The inert-gas flow was controlled by a constant-leak valve and monitored by the chamber pressure. Both the sample and inert-gas band intensities are similarly affected by the transmission efficiency of the analyzer and the sensitivity of the detector. The conversion of BR to RPPICS uses the published inert-gas photoionization cross sections[16] and adjusts for the variations in these instrumental factors.

The statistical errors are given by $(100n^{1/2}/n)\%$, where n is the number of observations. For band areas, n translates into the number of counts subsumed by the integrated band area. For example, for three bands of areas 1000, 3000, and 6000 counts, the derived BR and their errors would be $0.1 \pm 0.003/0.3 \pm 0.006/0.6 \pm 0.008$. For bands of areas 100, 300, and 600, the BR errors increase to $0.1 \pm 0.01/0.3 \pm 0.03/0.6 \pm 0.04$. In acquiring a spectrum, we ensured good counts by using a measurement interval of 0.02 or 0.025 eV and acquiring data until the maximum counts were in the 250−500 range. Frequently, at lower photon energies, they were in the thousands. The weakest peak was the f band in the $U(BH_4)_4$ spectra below 30 eV and at 96 eV below the 5d−5f resonance. At a photon energy of 20 eV, the counts for the f band area were 1200, and those for the ABC band were 30,000. At a photon energy of 96 eV, the counts for the f band area were 400, and those for the ABC band area were 1250. Thus, we conclude that the BR values are statistically significant with errors in BR in the large majority of spectra of $<\pm 0.001$, and even for the U compound in the worst case at a photon energy of 96 eV, the errors were less than ± 0.04.

The choice of the number of Gaussian peaks to fit the complex band structure ABC is arbitrary. Two gave a poor fit to the band profile, whereas with four, one band proved to be superfluous. Three were used, and the widths of B and C were fixed to ensure that they covered the same part of the band throughout. This procedure resulted in the positions of A, B, and C being consistent over the whole photon-energy range to within ± 0.04 eV.

Calculations. Density functional calculations were performed using the Amsterdam Density Functional code (version ADF2000.02).[17−19] The generalized gradient approximation was employed, using the local density approximation of Vosko, Wilk, and Nusair,[20] together with nonlocal-exchange correction by Becke[21] and the nonlocal-correlation corrections by Perdew.[22] TZ2P basis sets were used with triple-ζ accuracy sets of Slater-type orbitals, with two polarization functions added to the main group atoms. Relativistic corrections were made using the ZORA (zero-order relativistic approximation) formalism. IEs were obtained by direct calculations on the molecular ions in their ground and appropriate excited states and subtraction of the energy of the neutral molecule. Spin-orbit calculations, as available in the ADF program suite, were also carried out for $U(BH_4)_4$, for both the ground-state molecule and its molecular-ion states.

Results and Discussion

General Considerations. All three tetrakis-borohydride molecules have been structurally determined by gas-phase electron diffraction (GED): in each case, they are shown to adopt an η^3-BH_4 bonding mode. For $U(BH_4)_4$, a structure

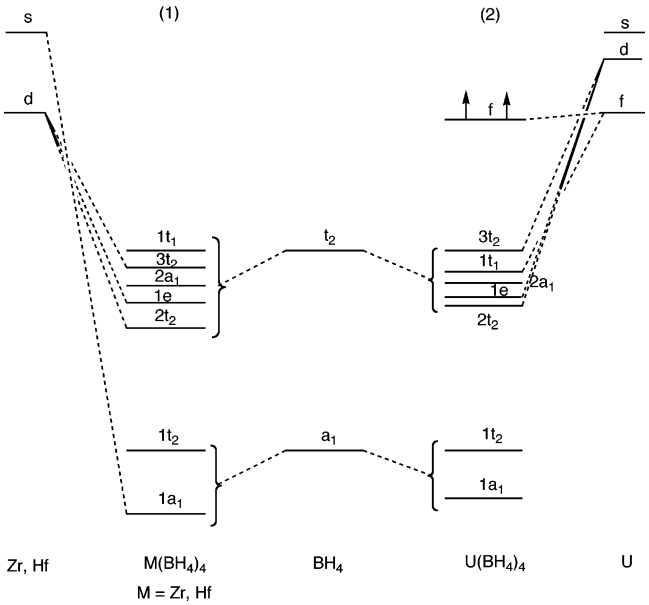

Figure 1. Schematic MO diagram for $M(BH_4)_4$ (1) where M = Zr or Hf and (2) M = U.

(16) Yeh, J. J. *Atomic and Nuclear Data Tables*; AT & T, Gordon Breach: Langhorne, PA, 1993.

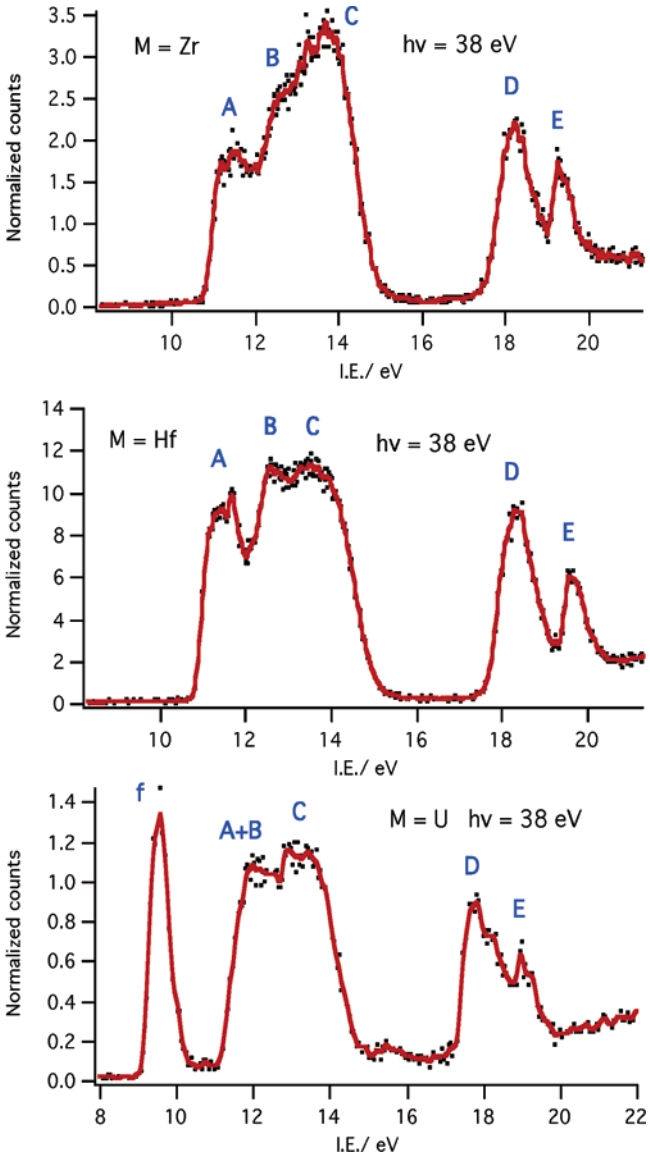

Figure 2. PE spectra of $M(BH_4)_4$ (M = Zr, Hf, and U), measured with hν = 38 eV.

with T_d molecular symmetry is favored, in which the three U−H−B bonds of each tetrahydroborate ligand are exactly staggered with respect to the opposing UB_3 fragment.[13] For $Zr(BH_4)_4$ and $Hf(BH_4)_4$,[13,23] these bridging M−H−B moieties are rotated from a staggered arrangement to give a molecular symmetry of *T* rather than T_d. However, the heavy-atom MB_4 core retains its T_d symmetry, and the MO schemes and PE spectra for these two molecules can be interpreted in this point group. Lowering the molecular symmetry from T_d to *T* in the transition-metal derivatives will have greatest effect

(17) *SCM*, version 2000.2; Theoretical Chemistry, Vrije Universiteit: Amsterdam, 2000.
(18) te Velde, G.; Bickelhaupt, F. M.; van Gisbergen, S. J. A.; Fonseca Guerra, C.; Baerends, E. J.; Snijders, J. G.; Ziegler, T. *J. Comput. Chem.* **2001**, *22*, 931.
(19) Fonseca Guerra, C.; Snijders, J. G.; te Velde, G.; Baerends, E. J. *Theor. Chem. Acc.* **1998**, *99*, 391.
(20) Vosko, S. H.; Wilk, L.; Nusair, M. *Can. J. Phys* **1990**, *58*, 1200.
(21) Becke, A. D. *Phys. Rev.* **1988**, *A38*, 2398.
(22) Perdew, J. *Phys. Rev.* **1986**, *B33*, 8822.
(23) Borisenko, K. B.; Downs, A. J.; Robertson, H. E.; Rankin, D. W. H.; Tang, C. Y. *Dalton Trans.* **2004**, 967.

Table 1. Ionization Energies of Valence and Core Levels of $M(BH_4)_4$ (M = Zr, Hf, and U)[a]

band		Zr		Hf		U
f						9.50
A		11.44		11.46		11.76
B		12.55		12.66		12.56
C		13.75		13.90		13.56
D		18.20		18.38		17.70
D′						18.24
E		19.33		19.72		18.97
core		**Zr**		**Hf**		**U**
B 1s		195.1		195.2		195.1
M	4p	37.9	4f	24.55	6p	27
		39.5		26.22		36
	3d	189.7	5p	40.2	5d	104
		192.1		47.2		113

[a] The valence IE compared with previously published data.[8,9] The values given for A, B, and C correspond to the average values for each of three Gaussian bands fitted to the PE spectra over the observed photon-energy range. The core ionizations, apart from the Hf 4f bands, have not been reported previously and are discussed in the section on core ionizations.

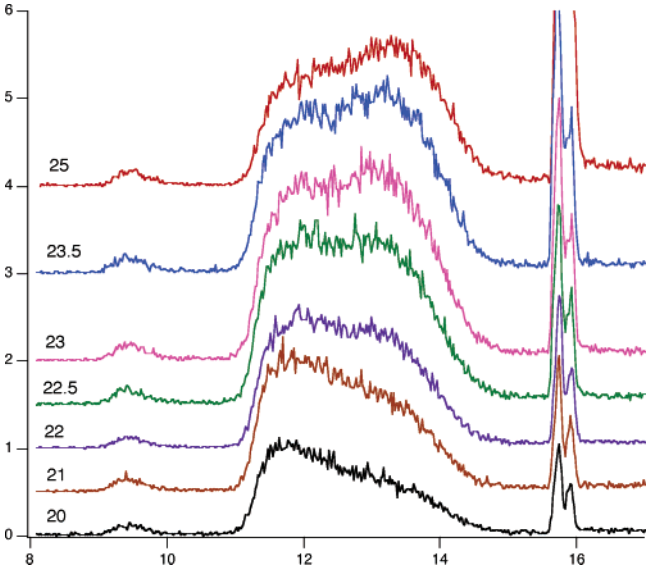

Figure 3. PE spectra of $U(BH_4)_4$ measured with photon energy = 38 eV. The $U(BH_4)_4$ spectra show also Ar bands.

on the $1t_1$ and $3t_2$ orbitals, which occur at similar binding energies (−8 to −9 eV): these will both now have t symmetry. However, as both of these MOs consist almost exclusively of localized BH_4 group orbitals composed of H 1s and B 2p contributions, the effects of this symmetry reduction on metal-ligand bonding will be minimal.

Figure 1 shows two MO schemes, assuming T_d symmetry, based on the DFT calculations described in more detail below; one is for the d-block compounds ($Zr(BH_4)_4$ and $Hf(BH_4)_4$) and the other is for the f-block one ($U(BH_4)_4$).

The valence PE spectra of all three molecules, measured with a photon energy of 38 eV, are shown in Figure 2. Ionization energies of the principal features are given in Table 1 and are in agreement with the literature data.[8,9]

The valence spectra of the Zr and Hf compounds show two regions labeled ABC and DE in Figure 2. These are associated with orbitals derived from the t_2 and a_1 orbitals of BH_4, respectively. The BH_4 t_2 orbitals are B 2p-based and

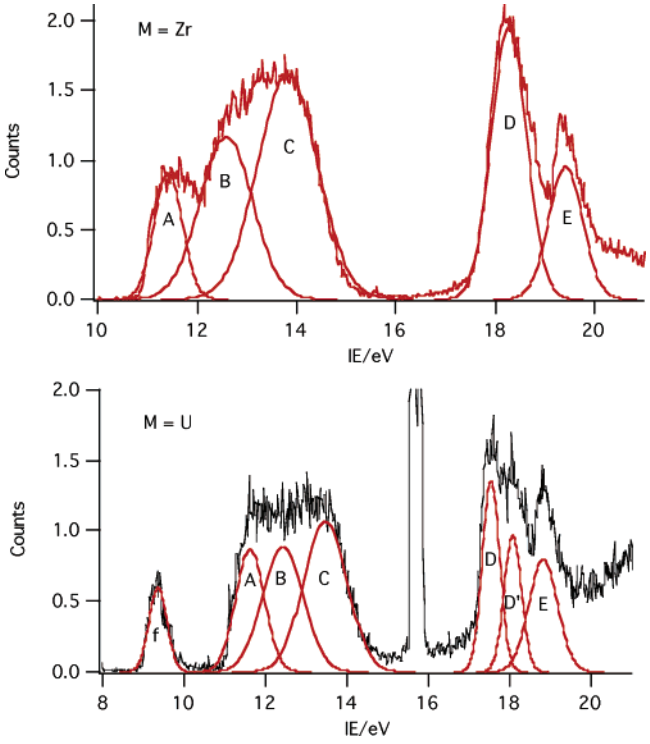

Figure 4. Examples of the fit of Gaussian peaks used to quantify the relative PE band intensities of $M(BH_4)_4$ (M = Zr and U). The $Zr(BH_4)_4$ spectrum was acquired with a photon energy of 31 eV and the $U(BH_4)_4$ spectrum with a photon energy of 33 eV. Ar is also present in the $U(BH_4)_4$ spectrum.

the a_1 orbitals are B 2s-based. The B 2p/B 2s AO separation is the major factor defining the primary energy separations in the valence spectrum.

The principal difference between the PE spectra of the d-block transition metal and the actinide derivatives is the presence of the f band in the latter. Another significant difference is that, for $Zr(BH_4)_4$ and $Hf(BH_4)_4$, the bands derived from the BH_4 t_2 orbitals are spread over a wider energy range. Band A is more distinct for these transition metal species, whereas for $U(BH_4)_4$ it appears to merge with band B. In the earlier PE studies,[7,8] band A was assigned differently for the Zr and Hf compounds; Downs et al.[8] assigned band A to the terminal B−H bonds, whereas Hitchcock et al.[9] assigned it to the t_1 band. Subsequent Xα-SW calculations supported the latter assignment, to the $1t_1$ band.[11]

Five primary ion states are assigned to feature ABC, and some of these are expected to undergo further splitting by Jahn−Teller distortion of the molecular ion. It was not realistic to attempt to fit band ABC with five Gaussian peaks. The ABC band shape, however, varied considerably over the photon-energy range. For example, Figure 3 shows the $U(BH_4)_4$ spectra in the 8−16 eV range for photon energies between 20 and 25 eV. The most satisfactory quantitative description of the profile variation required the use of three Gaussian peaks. For $Zr(BH_4)_4$ and $Hf(BH_4)_4$, the first, A, was fitted to the leading peak, and B and C were fitted to the high- and low-energy sides of the second band. The

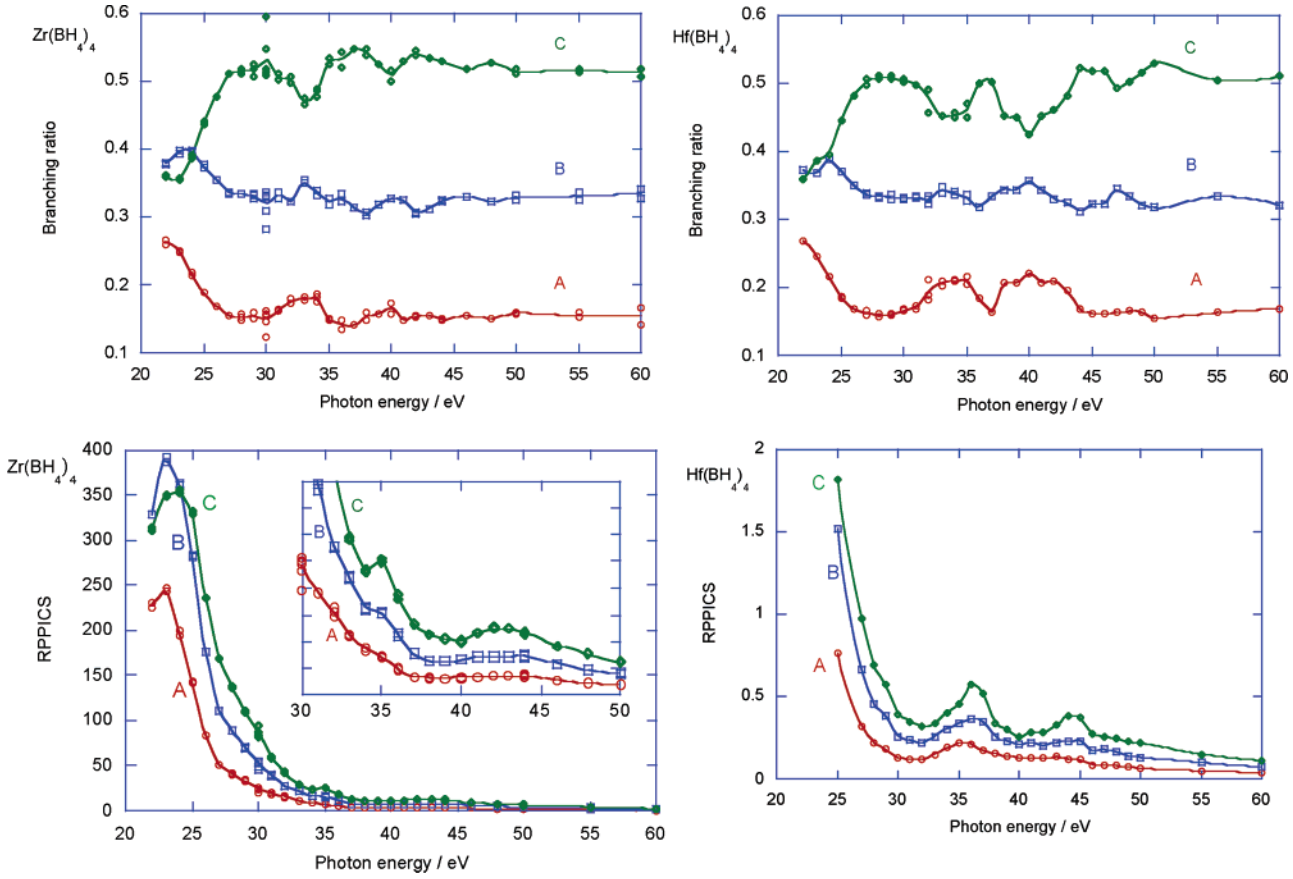

Figure 5. BR and RPPICS for the A, B, and C bands of $M(BH_4)_4$ (M = Zr and Hf).

widths of Gaussians B and C were constrained during the fits to ensure that they were comparing comparable IE ranges. For $U(BH_4)_4$, A, B, and C were fitted to the lower, middle, and upper regions of the band, again with the widths of B and C constrained. This procedure resulted in constant peak positions throughout the series of spectra for all three compounds. It should be stressed however that A, B, and C do not correspond to particular ion states, except probably band A in the cases of the Zr and Hf compounds. For $Zr(BH_4)_4$, D and E were fitted freely, while for its Hf analogue the width of E was fixed. In the case of $U(BH_4)_4$, band D was split, so two Gaussians (D and D′) were used and their widths were constrained along with that of E. Examples of fitted spectra for $Zr(BH_4)_4$ and $U(BH_4)_4$ are presented in Figure 4.

The band areas so derived and their relative intensity variations were expressed as BRs. Fitting of the noble-gas band areas enabled these BRs, in combination with the published noble-gas cross sections, to be converted into RPPICS. The RPPICS gives a measure of how the ionization probability varies with photon energy.

Branching Ratios and Relative Partial-Photoionization Cross Sections. Consideration of the changes in BR and RPPICS enables identification of the AO contributing to the MO from which an ionization is taking place.

Bands A, B, and C for M = $Zr(BH_4)_4$ and $Hf(BH_4)_4$. Figure 5 shows BR and RPPICS data for bands A, B, and C of $Zr(BH_4)_4$ and $Hf(BH_4)_4$. The RPPICS data are dominated by the decrease in ionization probability from H 1s and B 2p orbitals. Figure 6a gives calculated cross sections for these AOs, which show the steep decay of these cross sections with photon energy. There are other features apparent in the RPPICS plots, which are emphasized upon inspection of the BR as the decay with photon energy is common to all parts of the band.

$Hf(BH_4)_4$ shows maxima in the RPPICS at 36 and 44 eV. This is evident in all three RPPICS curves, but the BR plots show it to be strongest for band C. Their position and separation are consistent with these maxima resulting from 5p → 5d resonant excitation and SCK decay. The 5p subshell has IEs of 40.2 and 47.2 eV (Table 1), the resonant excitation occurs below these energies.

The BR plot for $Hf(BH_4)_4$ also shows rapid growth in the relative intensity of C at low photon energies. This is also attributable to d-orbital character, with Hf expected to show a delayed maximum and a relatively slow decay in its 5d cross section (Figure 6b).

For $Zr(BH_4)_4$, a 4p → 4d resonance is less visible but also present. Band C shows a maximum in its RPPICS at 35 eV; the 4d subshell ionizes at 37.9 and 39.5 eV (Table 1). The relative intensity increase at this photon energy is confirmed in the BRs for $Zr(BH_4)_4$. There is also a maximum in the band C RPPICS at 42 eV. This is too high an energy to be associated with the p−d resonant excitation.

The BR plots for $Zr(BH_4)_4$ in the low-IE region are very similar to those for its Hf congener. The early relative rise in the intensity of band C shows a 4d orbital contribution to the associated MOs (Figure 6b).

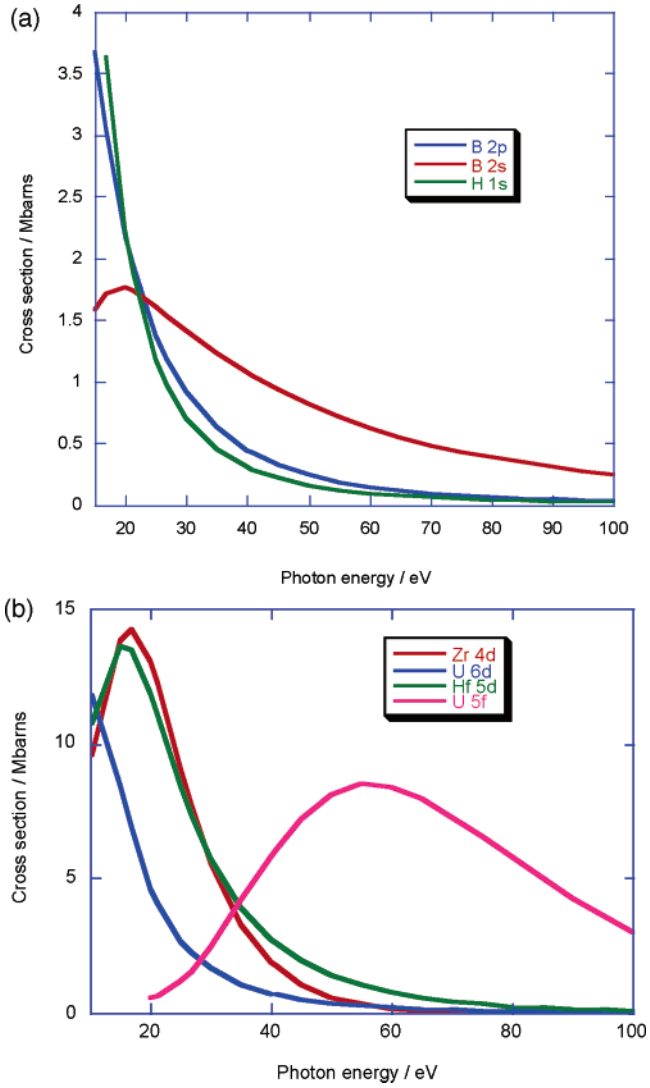

Figure 6. Calculated cross sections for (a) H 1s, B 2s, and B 2p orbitals and (b) Zr 4d, Hf 5d, and U 6d and 5f orbitals.[16]

Thus, for both $Zr(BH_4)_4$ and $Hf(BH_4)_4$, there is evidence of d-orbital covalency, with the metal d contribution concentrated in the MOs contributing to band C.

Bands f, A, B, and C for $U(BH_4)_4$. For $U(BH_4)_4$, the growth in intensity of the f band is evident in both the BR and the RPPICS plots shown in Figure 7. Between 30 and 35 eV photon energy, band A also shows a perceptible increase in BR when compared with that of bands B and C. This is consistent with an f-orbital contribution to the MOs that form this part of the band (Figure 6b).

However, interpretation of the low photon-energy region is complicated by the fact that the U 6p subshell ionizes at 27 and 36 eV (Table 1), so that bands with a 6d contribution may also show resonances in this range. The growth in the relative intensity of C between 20 and 27 eV photon energy (Figures 3 and 7) is greater than that found for the Zr and Hf derivatives and may well reflect a resonance contribution to the increase, in addition to the increase expected from the delayed maximum in the 6d cross section. The second part of the 6p → 6d resonance would coincide with the increase in the f-orbital cross section, making qualitative

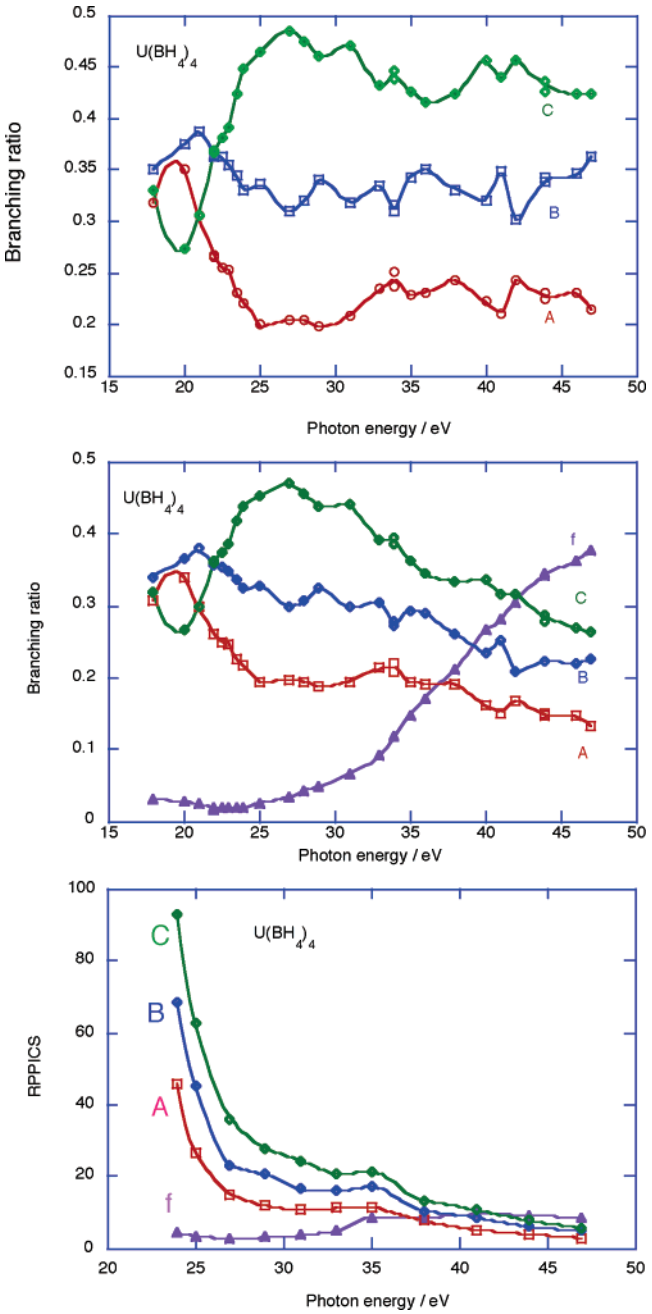

Figure 7. BR and RPPICS for the f, A, B, and C bands of $U(BH_4)_4$.

interpretation in this region complex. Indeed, all bands show an increase in their RPPICS around 35 eV. However, some support for an f-orbital contribution to the MOs associated with A is found in the value of the A/(A + B + C) BR at 40−45 eV, which is greater than 0.2. The corresponding BRs for $Zr(BH_4)_4$ and $Hf(BH_4)_4$ are around 0.15.

Branching Ratios of A + B + C versus D + E. The relative areas of bands A + B + C and D + E for all three molecules are shown in Figure 8. The statistical ratio of the number of orbitals contributing to the two bands is 3/1 (0.75 vs 0.25). The observed BR departs considerably from this. In each case, the intensity of bands D + E is very low near threshold, but their BR increases rapidly.

All three compounds show a clear maximum in the D + E BR and a corresponding minimum in that of A + B + C.

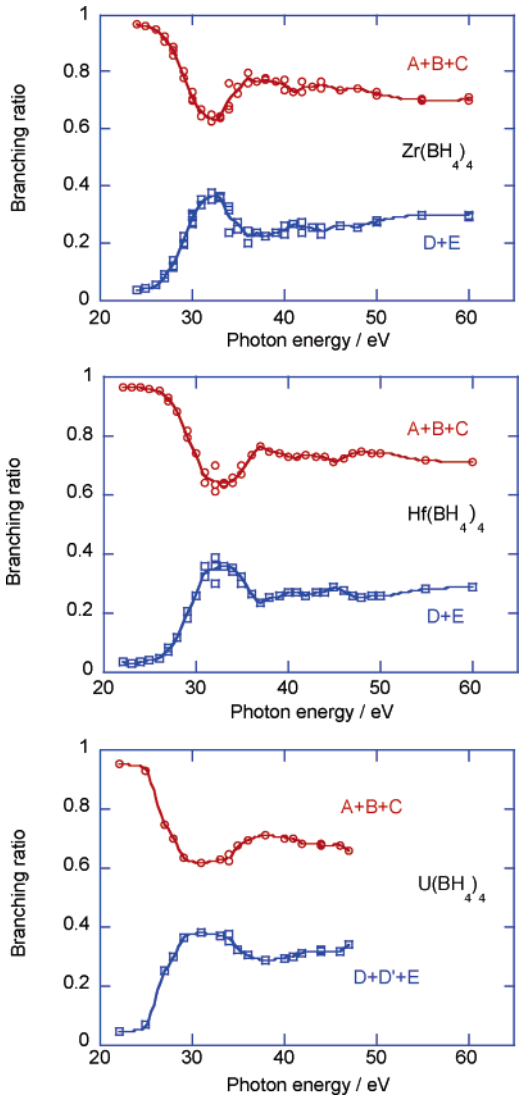

Figure 8. BR of A + B + C vs D + E for $M(BH_4)_4$ (M = Zr, Hf, and U).

For $Zr(BH_4)_4$ and $Hf(BH_4)_4$, this occurs at 32.5 eV. For $U(BH_4)_4$, the feature is somewhat broader and is centered at 31.2 eV. The cause of this feature is explored further below.

In the photon-energy range above 45 eV, the BR variations are less extreme; the values at photon energy 55 eV are $Zr(BH_4)_4$ 0.7/0.3, $Hf(BH_4)_4$ 0.72/0.28, and at 46 eV $U(BH_4)_4$ 0.68/0.32. The most probable cause of these lower than statistical 3/1 ratios is the differing cross-section variations of the B 2s and B 2p orbitals. The calculated values for these are shown in Figure 6a. The B 2s cross section decays less rapidly with photon energy than does that of B 2p. Thus, to the extent that bands A, B, and C are BH_4 t_2-based with B 2p character and bands D and E are BH_4 2s based, the ABC versus DE branching ratio should be less than the statistical value.

Bands D and E. Bands D and E for all three molecules show a strong resonance with a maximum between 30 and 35 eV (Figure 9). Though the exact position of this maximum varies according to the metal and to the band, it is clear that there is a strong shape resonance present in these bands, which is also the cause of the maximum in the D + E versus

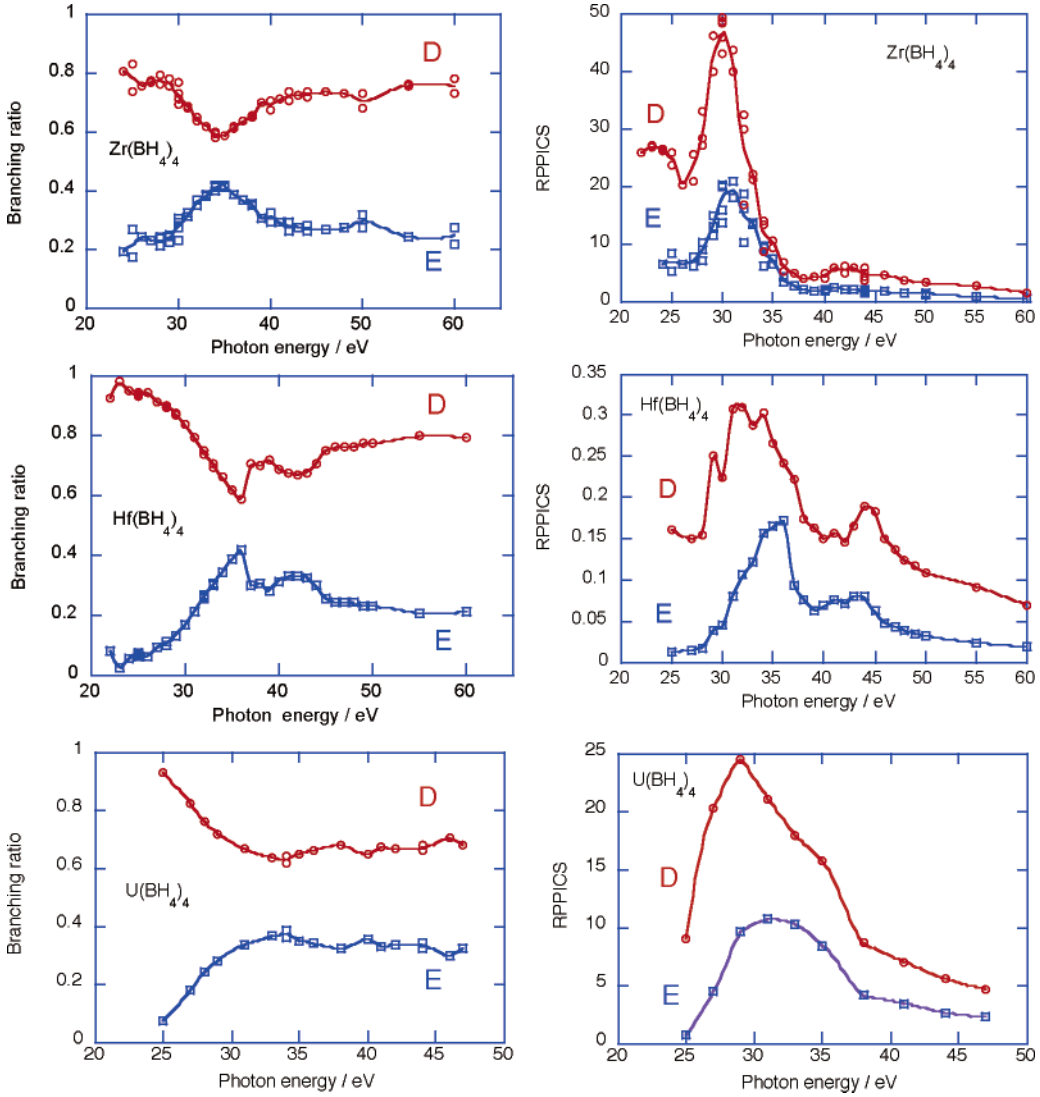

Figure 9. BR and RPPICS for bands D and E of $M(BH_4)_4$ (M = Zr, Hf, and U).

A + B + C BR discussed above. Tetrahedral molecules show shape resonances in their a_1 bands.[24] The presence of such a resonance in both the $1t_2$ and the $1a_1$ band suggests that it is an underlying feature of the BH_4 ligand. The D versus E BR shows that the resonance is stronger in the E $1a_1$ band than in the $1t_2$ one, so there is possibly an effect also from the overall T_d molecular symmetry or the shape resonance may be intrinsic in the $1a_1$ band and arise in the $1t_2$ band also as a result of interchannel coupling.

The D RPPICS of $Hf(BH_4)_4$ shows resonances at 36 and 44 eV. That at 44 eV is evident in the RPPICS. That at 36 eV overlays the upper region of the shape resonance but is visible as an increase in the D BR. Thus, a 5d contribution to the $1t_2$ MO may be deduced. For $Zr(BH_4)_4$ and $U(BH_4)_4$, p → d resonances are not detectable but may be present and masked by the shape resonance. For the latter molecule they could account for the apparent breadth of the shape resonance.

$U(BH_4)_4$ at High Photon Energies. At photon energies above 50 eV, shape resonances are not expected, and the effect of the p−d resonant excitations is absent. Thus, an examination of the 5d−5f resonance region can give less ambiguous evidence for 5f covalency. The U 5d shell ionizes at 104 and 113 eV, so a 5d → 5f resonance is anticipated in this region. The U f band shows massive intensity changes over the photon range of 90−120 eV. Figure 10 shows the PE spectrum of $U(BH_4)_4$ acquired with a photon energy of 108 eV. The RPPICS of the f band (Figure 11) shows two maxima at 98 and 108 eV, corresponding to $J = 5/2$ and 3/2 core holes.

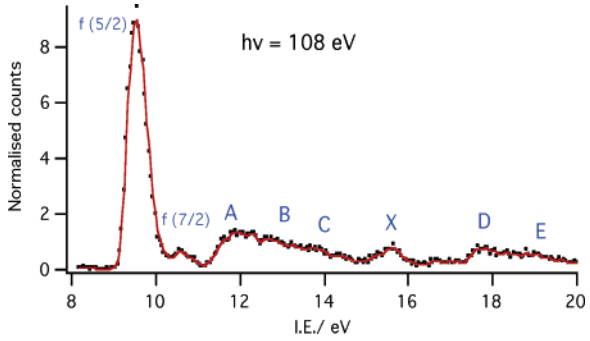

Figure 10. PE spectrum of $U(BH_4)_4$ at 108 eV.

(24) Green, J. C.; Decleva, P. *Coord. Chem. Rev.* **2005**, *249*, 209.

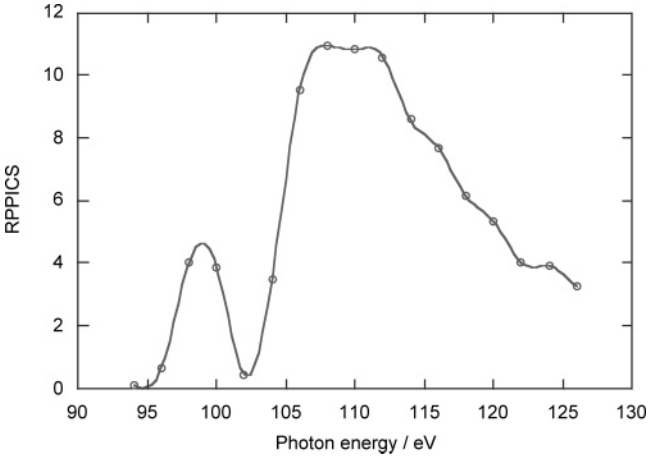

Figure 11. RPPICS of the f band of $U(BH_4)_4$ between 94 and 126 eV.

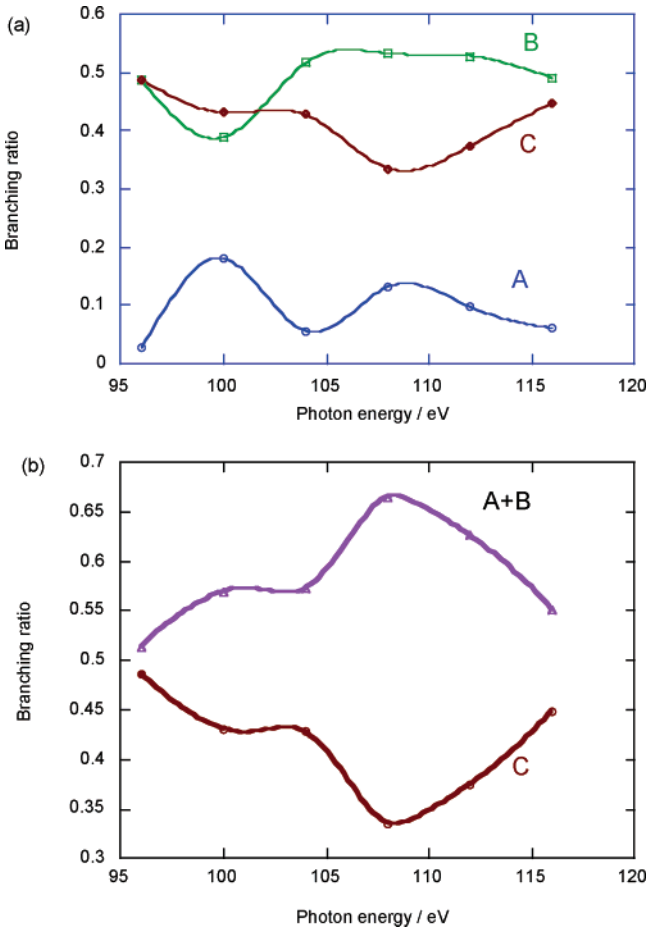

Figure 12. Branching ratios of bands A, B, and C of $U(BH_4)_4$ between 96 and 116 eV. Panel a shows the BR of A, B, and C separately normalized to the total ABC band area. Panel b shows the combined intensity of A + B relative to C.

The RPPICS of the other bands, A−E, are extremely low, but it was possible to obtain BR data on bands A−C to seek confirmation of f-orbital covalency. The low-energy half of the ABC band is visibly more intense than the high-energy part at photon energies corresponding to these maxima (eg., Figure 10). Figure 12a shows that band A has maxima in its BR at values corresponding to those of the f band. More strikingly, when the intensity of A and B combined is compared with that of C, the double-humped structure of the f resonance is clearly visible. In concert with the behavior of band A in the regions of the f-band delayed maximum, this confirms f-orbital covalency in the MOs contributing to the low-energy region of the ABC band.

Figure 10 shows two additional bands that become clearly visible in the resonance region. One at 10.45 eV is separated by 0.95 eV from the main f band, and can be assigned to the $^2F_{7/2}$ ion state. This gives a spin−orbit coupling constant of 0.27 eV (2200 cm^{-1}) for U(V) in line with literature values (1900−1925 cm^{-1}).[25,26] Its intensity compared to the $^2F_{5/2}$ band is 0.07/1. The $^2F_{7/2}$ ion state has a low probability of being accessed by direct photoemission as the coupling pattern for f electrons in U is closer to the j−j rather than the Russell−Saunders limit.[8] However, the selection rules for resonant photoemission differ and thus the higher spin−orbit component becomes accessible.

The other peak has an IE of 15.58 eV, which we assign to adventitious nitrogen.

Core Ionizations. To ascertain the likely positions for resonant transitions, we sought to identify the exact location of the core ionizations. Core ionizations were measured for B 1s ionizations in all three compounds, and for Zr 4p and 3d, Hf 4f and 5p, and U 6p and 5d ionizations. The measured IEs are given in Table 1. The constancy of the B 1s IE indicated that the charge on the BH_4 group was very similar for all three compounds.

In Figures 13 and 14, the photoelectron peaks from ionizations of the outer-core levels of metals are shown. For the Hf compound, we followed a fixed kinetic-energy structure moving through the Hf 5p bands for photon energies between 46 and 60 eV (Figure 13). The mean kinetic energy of the structure is 11.2 eV with a spread of almost 2.5 eV. Tentatively, we can assign this structure to an Auger decay process, $O_3N_{6,7}N_{6,7}$, with one electron from the 4f level ejected following the formation of the Hf $5p_{3/2}$ ionized state. To justify the kinetic energy of the structure, we must assume some relaxation of the orbitals upon formation of the ion.

In the Zr compound spectrum (Figure 14a) recorded at 60 eV, we observe a structure whose ionization energy might suggest assignment to Zr 4s (IE = 50.6 eV in metallic zirconium).[27] There are two arguments against this assignment. First, the chemical shift from the metallic values observed for the Zr 4p ionizations are around 10 eV, and those for the Zr 3d ionizations are 11 eV. This suggests that the Zr 4s orbital should ionize above 60 eV. Second, we observed a structure with a similar kinetic energy (KE ≈ 8.20 eV) in the spectrum recorded at 42.0 eV. In this case, we assign the structure to Auger molecular decay following the excitation of the Zr 4p levels.

The IEs of the $(n - 1)$p electrons lie a few eV higher than the maxima in the p to d resonances observed in the cross-section plots. The latter are indicative of the energies

(25) Karraker, D. G. *Inorg. Chem.* **1964**, *3*, 1618.
(26) Edelstein, N.; Brown, D.; Whittaker, B. *Inorg. Chem.* **1973**, *13*, 563.
(27) Sarma, D. D.; Rao, C. N. R. *J. Electron. Spec. Relat. Phenom.* **1980**, *20*, 25.

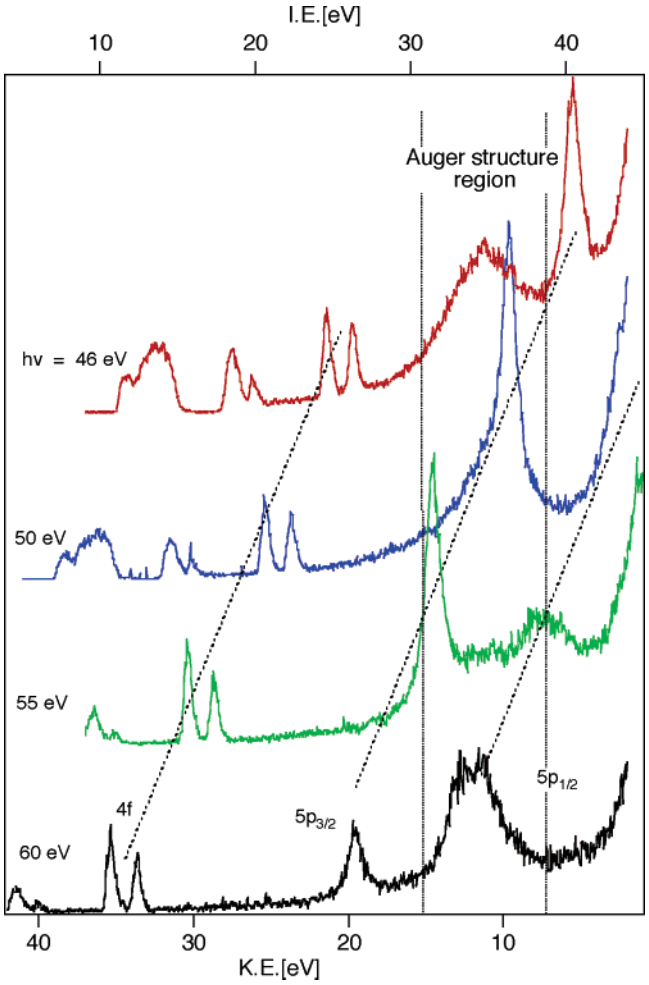

Figure 13. Core spectrum of $Hf(BH_4)_4$ at 46, 50, 55, and 60 eV, showing the 4f and 5p bands together with an Auger peak. The top x-axis refers to the highest spectrum, recorded at 46 eV.

required for p to d excitation, which involves less energy than p ionization.

Assignment of the U core spectrum (Figure 14b) is unambiguous.

Absorption Spectrum of $Zr(BH_4)_4$. In the case of $Zr(BH_4)_4$, it was possible to seek confirmation of both the 3p−3d resonant absorption and the shape resonance by recording its absorption spectrum. The absorption spectrum of $Zr(BH_4)_4$ was measured in the region of 24−60 eV (Figure 15). The 4p absorption edge shows a maximum at 35.5 eV, close to the maximum in the RPPICS of band C for this compound. Additional structure at 36.7 eV has a separation from the main peak of 1.2 eV, significantly less than the spin-orbit splitting of the core hole of 1.6 eV (Table 1). Thus, the most likely assignment of these two features is excitation to the unoccupied d levels of e and t_2 symmetry. Higher-energy structure is overlaid by ionization onset at 38 eV. However, it is noteworthy that the broad intense absorption centered at 41.3 eV coincides with the maximum in the band C RPPICS at around 42 eV.

Pre-edge structure can be distinguished at 32.5 and 33.8 eV. This absorption coincides with the shape resonance observed in bands D and E and can be related to that feature.

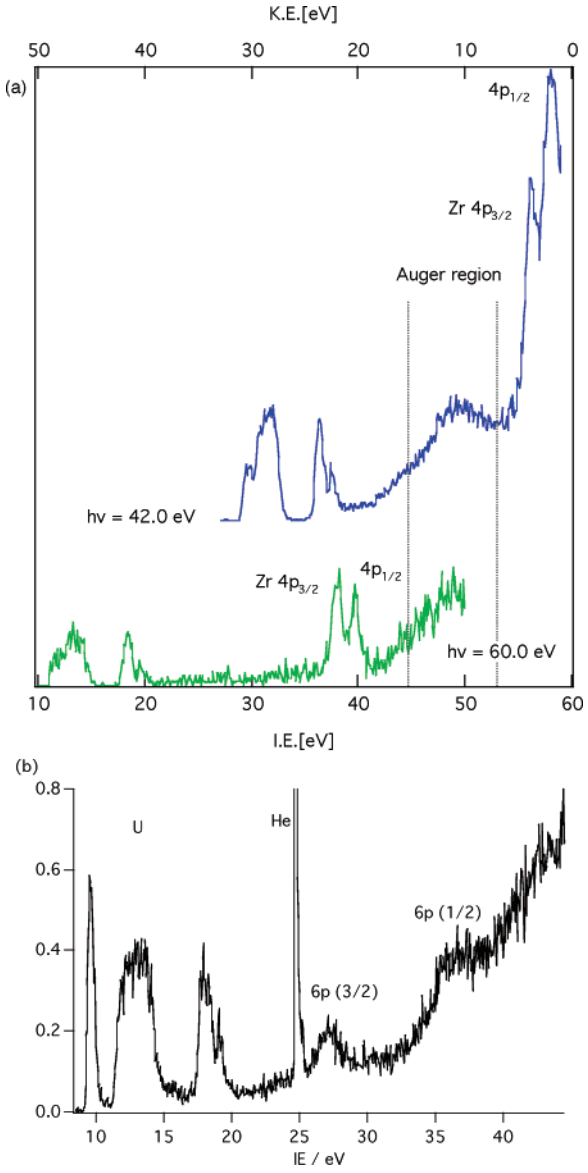

Figure 14. Core spectra of $M(BH_4)_4$ (M = (a) Zr and (b) U).

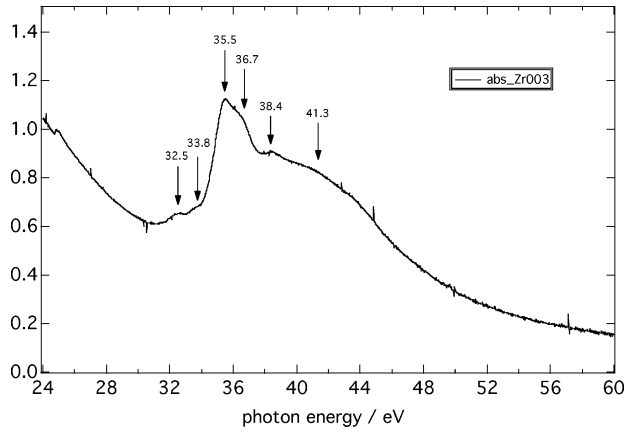

Figure 15. Absorption spectrum of $Zr(BH_4)_4$.

DFT Calculations. The gas-phase structure of $U(BH_4)_4$ as determined by GED indicates a molecule with T_d symmetry.[12,19] The GED structures of $Zr(BH_4)_4$ and $Hf(BH_4)_4$

Table 2. Calculated Distances (pm) for $M(BH_4)_4$ (M = Zr, Hf, and U), Assuming T_d Symmetry[a]

	Zr	Hf	U
B−H_t	119.7 (118.8)	119.6 (121)	119.7 (117.8)
B−H_b	125.3 (127.8)	125.2 (127.6)	126.1 (131.6)
M−H_b	210.9 (214.4)	210.7 (221.5)	223.2 (231.5)
M...B	227.4 (232.4)	227.1 (231.4)	243.3 (251.2)

[a] Experimental distances from GED are given in parentheses.[13,23,31]

Table 3. Kohn−Sham Orbital Energies, e_i (eV), and Calculated IE (eV) for $M(BH_4)_4$ (M = Zr, Hf, and U)

	Zr		Hf		U	
	e_i	IE	e_i	IE	e_i	IE
f					−5.21	8.44
					−5.51	8.74
$1t_1$	−8.44	10.97	−8.33	10.91	−9.09	11.53
$3t_2$	−8.86	11.29	−8.87	11.34	−8.55	10.87
$2a_1$	−9.3	11.73	−9.45	11.91	−9.25	11.59
2e	−9.84	12.35	−9.76	12.32	−9.71	12.14
$2t_2$	−10.39	12.88	−10.36	12.91	−9.89	12.27
$1t_2$	−13.95	16.57	−13.98	16.65	−13.61	16.12
$1a_1$	−15.1	17.6	−15.41	18.06	−14.75	17.26

indicate *T*, rather than T_d, molecular symmetry,[12,19] on account of the relative disposition of the M−H−B moieties. Rotation of the M(η^3-BH_4) units was found to be facile in each molecule, and hence T_d symmetry was assumed for all three $M(BH_4)_4$ molecules throughout.

The geometries of the three molecules were optimized. Calculated interatomic distances are in reasonable agreement with the experimental data (Table 2). IEs were calculated for ion states formed by creating a hole in the occupied valence orbitals and are reported in Table 3. The energy difference between ionizing α and β spin-orbitals for $U(BH_4)_4$ was so small that only the values for holes in the α spin-orbitals are reported.

Given the composite nature of the main band, it is not possible to make an exact comparison of the calculated and experimental values of IE for all the ion states. However, various points emerge when the values in Table 3 are compared with the band positions in Table 1. Overall, the agreement in absolute value is superior for the transition metal molecules than for their actinide congener. A comparison of the IE to the $^2T_1$ ion state with the vertical IE for band A shows a difference of 0.47 eV for $Zr(BH_4)_4$ and 0.55 eV for $Hf(BH_4)_4$, the calculated IE being the smaller. The difference increases with increasing IE, and for the $^2A_1$ IE and band E it is 1.63 eV for $Zr(BH_4)_4$ and 1.66 eV for $Hf(BH_4)_4$. For $U(BH_4)_4$, the difference for the $^2T_2$ ionization and band A is 1 eV and for the $^2A_1$ IE and band E 1.71 eV. However, given the general underestimates of IE, many features of the spectra are well reproduced by the calculations. The spacings of bands A, B, and C for all three compounds correspond well with the grouping of ion states associated with the BH_4 t_2 ionizations, with the separations for $U(BH_4)_4$ being significantly less than those for the Zr and Hf derivatives. For D and E, the assignments are clear-cut and the calculations reflect the lower IE for $U(BH_4)_4$ and the increase in the D−E separation for $Hf(BH_4)_4$ (1.34 eV experimental, 1.41 eV calculated) compared to $Zr(BH_4)_4$ (1.13 eV experimental, 1.03 eV calculated) and $U(BH_4)_4$ (1.09 eV experimental, 1.14 calculated).

Table 4. Percentage AO Contributions to the Occupied Valence MOs of $M(BH_4)_4$ (M = Zr, Hf, and U), Determined by Mulliken Population Analysis

		H 1s	B 2s	B 2p	M (n − 1)d	M ns	M np	M (n − 2)f	M (n − 1)p
Zr	$1t_1$	56		32					
	$3t_2$	55		31	2				
	$2a_1$	59	7	25		3			
	1e	45		28	23				
	$2t_2$	53		24	18				
	$1t_2$	54	28		7		6		
	$1a_1$	72	21			19			
Hf	$1t_1$	56		32					
	$3t_2$	56		28	2				
	$2a_1$	56	7	27		2			
	1e	44		28	23				
	$2t_2$	49		25	19				
	$1t_2$	53	27		7		7		
	$1a_1$	73	22			16			
U	f							96	
	$1t_1$	50		26				13	
	$3t_2$	58		31					
	$2a_1$	57	5	32					
	1e	54		24	18				
	$2t_2$	61		23	14				
	$1t_2$	55	26		8		3		3
	$1a_1$	78	24						

Orbital Compositions. Mulliken population analysis of the orbitals gives the atomic contributions shown in Table 4. Iso-surfaces of the analogous MO in $Zr(BH_4)_4$ and $U(BH_4)_4$ are compared in Figure 16. Figure 17 shows the iso-surfaces for the two f orbitals assigned to the unpaired electrons in $U(BH_4)_4$.

The $1t_1$ orbital is strictly nonbonding in $Zr(BH_4)_4$ and $Hf(BH_4)_4$; this accounts for the separation of band A from bands B and C in the spectra. For $U(BH_4)_4$, there is a significant 5f contribution which lowers $1t_1$ in energy, placing it below the $3t_2$ orbital. In the PE spectrum of $U(BH_4)_4$, this is reflected in the merging of band A with band B. The 5f contribution is also verified by the increase in RPPICS of A relative to B and C from 30 to 47 eV and for the resonant enhancement of band A + B compared with C in the 95−120 eV resonance region. In the spectral fitting, Gaussian peaks A and B overlap. The calculation suggests that the onset of band ABC is assignable to the $3t_2$ band and that the $1t_1$ ionization is adjacent. This concurs with the combination of bands A and B tracking the f band better than A on its own. The calculation suggests a 13% 5f contribution to the $1t_1$ MO.

The 1e and $2t_2$ MOs have significant metal d character. The percentage contribution is similar for the Zr and Hf compounds, and slightly lower for the U one. These contributions are verified experimentally by the (n −1)p to (n − 1)d resonances observed in the cross sections.

The $1t_2$ MOs are nodally better suited to overlap with the metal p orbitals, which make a small contribution to these MOs. For $U(BH_4)_4$, mixing occurs both with the valence 7p orbitals and with the semi-core 6p orbitals. This latter component, although small, is the origin of the spin−orbit splitting of band D observed for this molecule.[28,29]

The metal s orbital is calculated to make a significant contribution to the $1a_1$ MOs for $Zr(BH_4)_4$ and $Hf(BH_4)_4$ (the

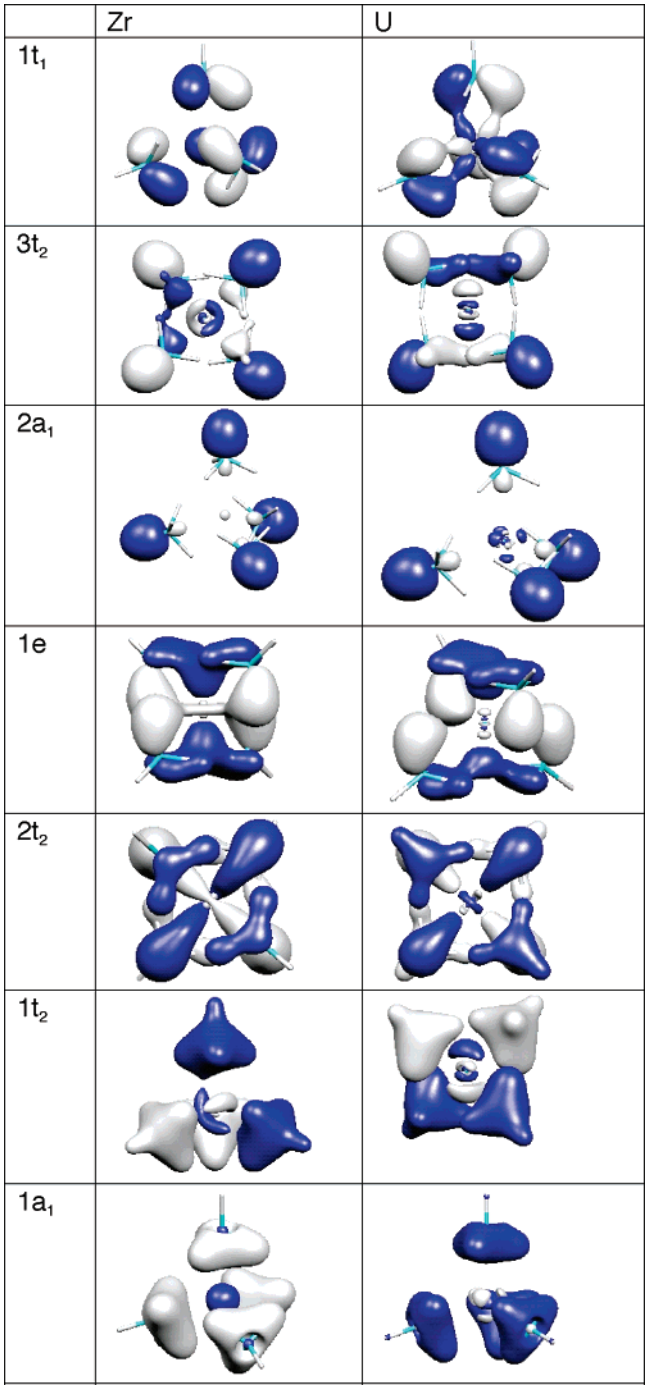

Figure 16. Isosurfaces of the valence MOs of $M(BH_4)_4$ (M = Zr and U).

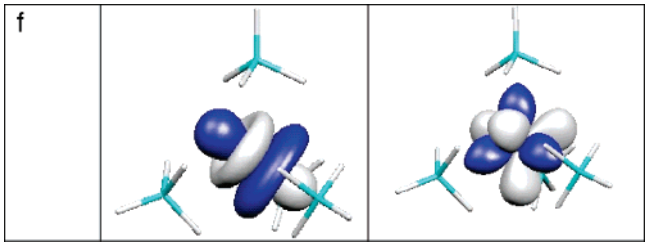

Figure 17. Populated f orbitals of $U(BH_4)_4$.

surface observed around Zr in Figure 16 for the $1a_1$ MO is an inner lobe of the 4s orbital). The 6s contribution for Hf is slightly less than the 5s contribution for Zr; the greater stability and higher IE for the $1a_1$ orbital for $Hf(BH_4)_4$ is accounted for partially by the relativistic stabilization of the 6s orbital.[30] For $U(BH_4)_4$, the percentage of 7s contribution is negligible. Its diffuse nature gives it very little overlap with the ligand orbitals.

The calculations provide excellent support for the deductions made from the cross-section analysis and the energies and splittings of the PE bands.

Table 5. Comparison of Orbital Energies (eV) of $U(BH_4)_4$ With and Without Spin−Orbit Coupling

without spin−orbit coupling		with spin−orbit coupling	
orbital symmetry	energy	energy	orbital symmetry
f	−5.21, −5.51	−5.16	$e_{1/2}$
$3t_2$	−8.55	−8.44	$u_{3/2}$
		−8.89	$e_{5/2}$
$1t_1$	−9.09	−9.10	$u_{3/2}$
		−9.11	$e_{1/2}$
$2a_1$	−9.25	−9.31	$e_{1/2}$
1e	−9.71	−9.76	$u_{3/2}$
$2t_2$	−9.89	−9.90	$u_{3/2}$
		−10.02	$e_{5/2}$
$1t_2$	−13.61	−13.47	$u_{3/2}$
		−13.99	$e_{5/2}$
$1a_1$	−14.75	−14.79	$e_{1/2}$

Spin−Orbit Calculations. Calculations on $U(BH_4)_4$ were carried out using the spin-orbit methodology incorporated in the ADF program suite. In Table 5, the orbital energies calculated with and without spin-orbit coupling are compared. The spin-orbit calculation assigns the two f electrons to an $e_{1/2}$ orbital. Little variation is found in the orbital energies between the two methods. The $1t_2$ orbital is split by 0.52 eV into $u_{3/2}$ and $e_{5/2}$ components, in good agreement with the 0.54 eV separation between the D and D′ PE bands of $U(BH_4)_4$.

Conclusions

The combination of variable photon-energy PE spectroscopy and density functional calculations have provided a detailed experimentally verified analysis of the bonding in the tetrahedral or *pseudo*-tetrahedral molecules $M(BH_4)_4$, (M = Zr, Hf, and U). Covalent interactions with the metal d orbitals are found for the 1e and $2t_2$ MOs and are also indicated for the $1t_2$ MO. For $U(BH_4)_4$, f covalency is also demonstrated, with the U 5f orbitals making a small but significant contribution to the $1t_1$ MO. This covalency stabilizes the $1t_1$ MO in $U(BH_4)_4$ compared with its Zr and Hf analogues, in contrast to other comparable IEs which are, in general, lower for the actinide molecule.

The U f band shows striking resonant enhancement in the 5p−5d resonant region, and resonant photoemission to the normally unobserved $^2F_{7/2}$ ion state is evident.

The splitting of the $1t_2$ band of $U(BH_4)_4$ is attributed to a small contribution of U 6p semicore electrons to this MO.

(28) Green, J. C.; Guest, M. F.; Hillier, I. H.; Jarrett-Sprague, S. A.; Kaltsoyannis, N.; MacDonald, M. A.; Sze, K. H. *Inorg. Chem.* **1992**, *31*, 1588.
(29) Bursten, B. E.; Green, J. C.; Kaltsoyannis, N. *Inorg. Chem.* **1994**, *33*, 2315.
(30) Kaltsoyannis, N. *J. Chem. Soc., Dalton Trans.* **1997**, 1.
(31) Broach, R. W.; Chuang, I.-S.; Marks, T. J.; Williams, J. M. *Inorg. Chem.* **1983**, *22*, 1081.

Acknowledgment. We thank the EU for financial support, which enabled the use of the ELETTRA synchrotron at Trieste. Part of this work has been carried out using the computational resources of the facilities of the Oxford Supercomputing Centre. We acknowledge the provision of studentships from the EPSRC and King's College London (H.M.I.P. and A.J.). We are grateful to Prof. Geoff Cloke for providing a sample of UCl_4.

IC050370U